The Effect of the Surface Composition on Electronic Properties of Methylammonium Lead Iodide Perovskite

ARTICLE · JULY 2015

DOI: 10.1016/j.jmat.2015.07.005

7 AUTHORS, INCLUDING:

Zhen-Kun Tang

Beijing Computational Science Research C…

16 PUBLICATIONS **21** CITATIONS

SEE PROFILE

Chiyung Yam

Beijing Computational Science Research C…

57 PUBLICATIONS **782** CITATIONS

SEE PROFILE

Li-Min Liu

Beijing Computational Science Research C…

100 PUBLICATIONS **1,059** CITATIONS

SEE PROFILE

Available online at www.sciencedirect.com

ScienceDirect

Journal of Materiomics 1 (2015) 213–220

www.ceramsoc.com/en/

www.journals.elsevier.com/journal-of-materiomics/

Effect of surface composition on electronic properties of methylammonium lead iodide perovskite

Wei Geng [a], Chuan-Jia Tong [a], Zhen-Kun Tang [a], ChiYung Yam [a], Yan-Ning Zhang [a,b], Woon-Ming Lau [a,b], Li-Min Liu [a,*]

[a] *Beijing Computational Science Research Center, No. 10 Dongbeiwang West Road, Haidian District, Beijing, 100094, China*
[b] *Chengdu Green Energy and Green Manufacturing Technology R&D Center, Chengdu, Sichuan, 610207, China*

Received 21 May 2015; revised 9 July 2015; accepted 15 July 2015
Available online 23 July 2015

Abstract

Methylammonium lead iodide perovskite, $CH_3NH_3PbI_3$, is one of the most promising photovoltaic materials for low-cost and clean source of energy. In this work, the first-principles calculations were carried out to investigate the different composition of $CH_3NH_3PbI_3$ (001), including both methylammonium iodide terminated (MAI-T) and PbI_2 terminated (PBI_2-T) surfaces. The calculated surface energies show that the MAI-T is thermodynamical more stable than the PBI_2-T one under the equilibrium growth condition. The electronic properties of the two types of surfaces are also different. The band gap of PBI_2-T is obviously smaller than that of MAI-T due to the surface Pb states. Band gaps of MAI-T decrease with increasing thickness, while band gaps of PBI_2-T are insensitive to the slab thickness. The calculated optical absorption coefficients suggest that both terminations are effective solar energy absorbers in the visible light spectrum.

Keywords: $CH_3NH_3PbI_3$; DFT; Surface; Electronic property

1. Introduction

Organic–inorganic hybrid perovskites, such as $CH_3NH_3PbI_3$, are becoming one of the most promising materials for sunlight energy conversion because of their high efficiency, low cost, easy preparation and solution processability [1,2]. Since their first use as sensitizing materials in 2009 by Kojima et al., $CH_3NH_3PbI_3$ has attracted increasing attentions and makes extremely fast progress in photovoltaic applications [3–8]. Currently, the power conversion efficiency (PCE) of perovskite-based solar cells reach rapidly to nearly 20% [9]. Several kinds of fabrication techniques were used to prepare perovskite solar cells with both mesoporous and thin-film device architectures. Perovskites are interfaced with various electron transport materials (such as C_{60}/PCBM [10,11], graphene/TiO_2 nanocomposites [12], nano-crystalline anatase/rutile TiO_2 [13,14] and ZnO [15]) and hole transport materials (such as organic molecules Spiro-OMeTAD, PEDOT:PSS [16] or inorganic CuI [17], CuSCN [18]) in these different configuration of solar cell. In a mesoscopic-structure solar cell, additional interface arises during perovskites are deposited onto a mesoporous network of optically inert scaffold oxide (TiO_2, Al_2O_3 [19] or ZrO_2 [20]). The high PCE can be achieved by different functioning device of perovskite solar cell, which implies the complexity and versatility of the selective contacts in efficient charge separation [21–25]. The intrinsic mechanism behind remains poorly understood at this stage. It is thus important to investigate the structural, electronic and optical properties of various perovskite surfaces.

Many theoretical efforts also have been devoted to study bulk $CH_3NH_3PbI_3$ perovskites using density functional theory

* Corresponding author. Tel.: +86 10 5698 1827.
E-mail addresses: gengwei@csrc.ac.cn (W. Geng), limin.liu@csrc.ac.cn (L.-M. Liu).
Peer review under responsibility of The Chinese Ceramic Society.

http://dx.doi.org/10.1016/j.jmat.2015.07.005

(DFT), and the mechanism of energy conversion in $CH_3NH_3PbI_3$ perovskite based solar cell have been widely discussed [26–37]. However, there are relatively few reports on the theoretical studies of $CH_3NH_3PbI_3$ surfaces. The (001) surface is one of the most common surfaces of $CH_3NH_3PbI_3$ perovskite, meanwhile the structural cell parameters matches with various TiO_2 surfaces. Because of the different terminations, the $CH_3NH_3PbI_3$ perovskite (001) generally has two kinds of surfaces. One is terminated by the methylammonium ($CH_3NH_3^+$, hereafter abbreviated as MA^+) iodide, and the other is terminated with the PbI_2. In the previous work, the PbI_2 terminated surfaces are carefully considered with and without vacancy, and the results suggested that the flat termination rather essential for the performance of perovskite-based solar cells [38]. In order to further know whether the other surface terminated of MA^+ is thermodynamical stable, it is necessary to know which kind of surface is more stable in the experimental conditions.

In this study, the atomics structure, stability and the electronic structure of the $CH_3NH_3PbI_3$ perovskite (001) are systematically explored by first-principles calculations. The results show that both terminated surfaces are thermodynamical stable at room temperature. Surprisingly, the surface terminated with MA^+ is more stable than the one with PbI_2. Meanwhile, the band gap of these two different terminations show distinct features. The band gap of the surface terminated with MA^+ is dependent on the slab thickness, while the band gap of the other does not show obvious relationship with the number of layers. The calculated optical absorption coefficients suggest that both terminations are effective solar energy absorbers in the visible light spectrum.

2. Computational details

The DFT calculations were performed using the Vienna Ab Initio Simulation Package (VASP) code [39,40]. The electron–ion interaction was described by the projector augmented wave (PAW) method [41–43]. Electronic orbitals 5*d*6*s*6*p*, 5*s*5*p*, 2*s*2*p*, 2*s*2*p* and 1*s* were considered as valence orbitals for Pb, I, C, N and H atoms, respectively. The cutoff energy 400 eV was used, and the *k*-space integration was done with a 4 × 4 × 1 *k*-mesh based on the Monkhorst–Pack scheme [44]. All the structures considered in this study were relaxed with conjugate-gradient algorithm until the forces on the atoms were less than 0.01 eV/Å. Periodic boundary conditions were applied in all three dimensions. Due to large sizes of Pb and I ions, cages formed by four PbI_6 octahedrons are large enough to accommodate MA^+ ions and there is no obvious chemical bond formation between MA^+ ions and the inorganic matrix. Therefore, the non-local density functional with van der Waal (vdW) correction, vdW-DF [45], was employed for the weak interaction in the system, as implemented in VASP by J. Klimeš et al. [46,47]. In this method, the semilocal generalized gradient approximation (GGA) correlation term is replaced by the nonlocal form of "vdW correlation" ($E_c^{LDA} + E_c^{nl}$ correlation energy), so the exchange-correlation energy takes the form of

$$E_{xc} = E_x^{GGA} + E_c^{LDA} + E_c^{nl} \quad (1)$$

Here, the Perdew–Burke–Ernzerhof (PBE) [48] exchange functional was employed. Born-Oppenheimer molecular dynamics (BOMD) were performed to study thermodynamic stability of various pervoskite surfaces using QUICKSTEP module in the CP2K Package [49]. A hybrid Gaussian and plane waves (GPW) basis sets were used where the Kohn–Sham orbitals are expanded in an atom centered Gaussian basis functions while the electronic charge density is described using an auxiliary plane wave basis. The valence electrons are treated with a double-ζ valence basis set with one set of polarization functions, i.e., DZVP basis set [50], whereas the core electrons and nuclei are represented using an analytical dual-space pseudopotential of Goedecker, Teter, and Hutter (GTH) [51]. We carried out the simulations in the NVT ensemble at 300 K using a Nose–Hoover thermostat. The total simulation time was 15 ps with time step of 1 fs.

3. Results and discussion

3.1. The surface structures with the different terminations

$CH_3NH_3PbI_3$ has two typical crystal structures: the tetragonal phase at room temperature and the orthorhombic phase at low temperature (<162 K). Considering the tetragonal phase is more stable than the orthorhombic phase under the ambient condition, we only examine the surface of the tetragonal phase in the following. As shown in Fig. 1(a), in the bulk $CH_3NH_3PbI_3$, each Pb atom coordinates to six I atoms, with four I atoms in the equatorial direction and two I atoms in the apical direction. The four dipolar organic MA^+ ions are in the octahedron PbI_6-cages. The calculated lattice constant of $a = b = 8.80$ and $c = 12.69$ Å agrees with the pervious XRD experimental result [52]. The initial orientation of MA^+ ions starts in a way with C–N bonds parallel to each other based on our previous work, which shows this orientation is in line with the experimental results at room temperature [53].

In this work, the (001) surface of $CH_3NH_3PbI_3$ perovskite is considered, considering the $CH_3NH_3PbI_3$ contains by the PbI_2 and CH_3NH_3I units, which is built along the (001), thus the (001) surface should have the relatively small surface energy. The (001) surface of ABX_3 perovskite has two types of surfaces: one is terminated with MA^+ and I^- ions (MAI-T), and the other is terminated with Pb^{2+} and I^- ions (PBI_2-T). It should be noted that MAI and PbI_2 are two precursors used in synthesis of $CH_3NH_3PbI_3$. Here, we constructed the perovskite slab models with the different number of layers, from single to five layers, along the (001) direction of perovskite bulk supercell, including a vacuum layer of more than 20 Å. The atoms and cell parameters are fully relaxed.

The optimized configurations of the two types with five-layer slabs are shown in Fig. 1(c). The MAI-T surfaces terminated with MA^+ and I^- ions are constructed by cutting a PbI_6 octahedron along the *c* direction as one layer. The PBI_2-T

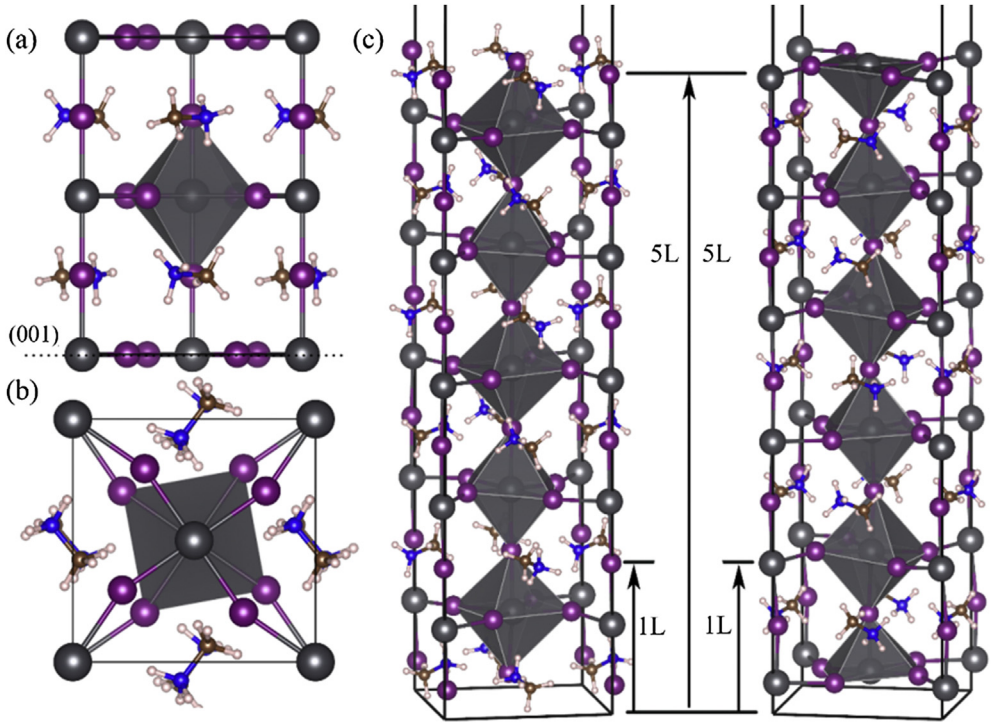

Fig. 1. The (a) side- and (b) top-views of bulk $CH_3NH_3PbI_3$ perovskite. (c) The optimized stable geometrical structures of 5-layer slabs with (001) surface of $CH_3NH_3PbI_3$ perovskite, left are MAI-T and right are PBI_2-T surfaces (dark gray: lead; purple: iodine; brown: carbon; blue: nitrogen; pink: hydrogen).

surfaces terminated with Pb^{2+} and I^- ions contains two opposing PbI_5 pyramid, namely two half of PbI_6 octahedron, which are cut as one layer.

In order to decrease the surface energy and stabilize the surface, the outermost layers of both types surface is reconstructed by the rotation of the PbI_6 octahedron and MA^+ ions. As shown in Fig. 1, the surface MA^+ ions of MAI-T surface reorient compared with the one in the inner layer, resulting in that the surface NH_3 groups point inwards while surface CH_3 groups point outwards. This demonstrates the interaction between ammonium hydrogen atoms and inorganic matrix [53].

3.2. The relative stabilities of the surface structures with different terminations

In order to know which kind of $CH_3NH_3PbI_3$ surface is more stable under the experimental conditions, the thermodynamical stability is firstly considered. Under the growth conditions of $CH_3NH_3PbI_3$ in the thermodynamic equilibrium, the existence of $CH_3NH_3PbI_3$ should satisfy:

$$\mu_{MA} + \mu_{Pb} + 3\mu_I = \Delta H_f^{MAPbI_3} \tag{2}$$

where μ_i is the chemical potential of chemical species, i, refers to their corresponding stable phase. $\Delta H_f^{MAPbI_3}$ is the formation enthalpy of $CH_3NH_3PbI_3$. In order to avoid the formation of possible secondary phases, such as PbI_2 and CH_3NH_3I, the following constraints must also be satisfied:

$$\mu_{MA} + \mu_I < \Delta H_f^{MAI} \tag{3}$$

$$\mu_{Pb} + 2\mu_I < \Delta H_f^{PbI_2} \tag{4}$$

To satisfy equations (2)–(4), the chemical potentials of Pb and I are limited in a narrow and long region as shown by red color in Fig. 2(a). This range indicates the equilibrium growth conditions for synthesizing $CH_3NH_3PbI_3$ phase. The yellow region on the upper right in Fig. 2(a) indicates the PbI_2-rich environment; on the contrary, the blue region on the lower left corresponds to a MAI-rich environment. The relation of chemical potential indicates that the growth conditions should be carefully controlled in the synthesis of $CH_3NH_3PbI_3$ perovskites. Our result is similar to the previous calculated chemical potentials for $CH_3NH_3PbI_3$ perovskites [32,34].

It is well known that the morphology and architecture of the light harvester significantly affect the performance of the solar cells. The balance between surface energy and epitaxial strain, and between energetics and kinetics, often controls surface morphology and facet growth in epitaxial films, as well as nucleation and growth of nanostructures. Here, the slab models in our study contain equivalent top and bottom surfaces with different stoichiometry from the bulk. In order to determine the relative stability of both terminations, the surface energies were calculated by chemical potentials of the constituent element:

$$E_{sur} = \frac{1}{2}\left[E_{slab}^{MA_\alpha Pb_\beta I_\gamma} - \alpha(E_{MA} + \mu_{MA}) - \beta(E_{Pb} + \mu_{Pb}) - \gamma(E_I + \mu_I)\right] \tag{5}$$

where E_{sur} is the surface energy, E_i is the energy of chemical species i in its stable phase, $E_{slab}^{MA_\alpha Pb_\beta I_\gamma}$ is the calculated total

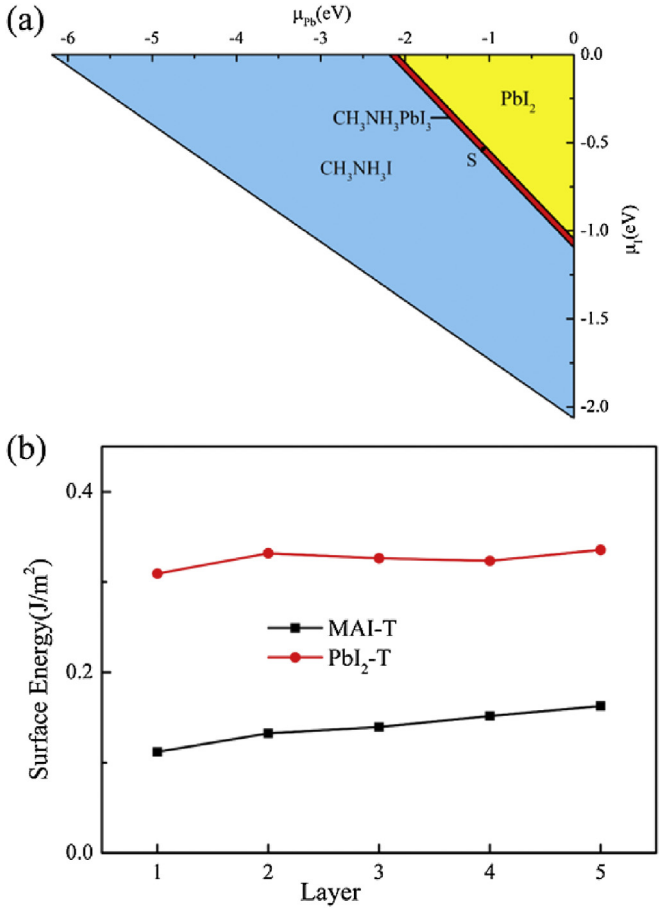

Fig. 2. (a) Thermodynamical stable range of Pb and I chemical potentials under the equilibrium growth condition of $CH_3NH_3PbI_3$. (b) The calculated surface energy of the MAI-T and PBI_2-T as a function of the number of layers.

energy of the slab. The surface energies depend on the chemical potentials of the constituent elements. In order to evaluate the surface energies, a moderate condition for reactants MAI and PbI_2 is chosen in this work, and the chemical potentials of μ_{Pb} and μ_I are 1.08 and 0.54 eV, respectively. The corresponding point is labeled as S at the red region in Fig. 2(a).

The calculated surface energies as a function of layer numbers for the two types of slabs in this condition are shown in Fig. 2(b). The calculated surface energies of MAI-T slabs are 0.11, 0.13, 0.14, 0.15 and 0.16 J/m^2 from one to five layers, and those of PBI_2-T slabs are 0.31, 0.33, 0.33, 0.32 and 0.34 J/m^2, respectively. Thus the surface energy gradually converges as the increase the number of layers, and the PBI2-T has the relatively larger surface energy than MAI-T. For PBI_2-T surface, every atom is connected with other atoms by chemical bond within the xy plane, thus the atomic movement of surface atoms within the xy plane become difficult. For MAI-T surface, the MA ions interact with inorganic cage by weak interactions, thus they could rotate in the cage, and I atoms have no bonding along xy plane but only one bond along Z direction. The different chemical bonding results in the distinct relaxation of the two surface terminations. Because of rotation of the MA+, the surface energy of MAI-T is relatively lower than the other.

The MAI-T surfaces are thermodynamical more stable than PBI_2-T ones, showing that MAI-T surfaces are favorable during equilibrium growth of $CH_3NH_3PbI_3$ pervoskites. The PbI_2-T surface could form only under the PbI_2-rich condition. Due to its relatively larger surface energy, the binging energy between PbI_2-T surface and electron and hole transport materials surface or molecules are stronger than that of MAI-T surface. However, the PbI_2-rich condition may induce the coexistence of secondary PbI_2 phases. Previous experimental works have observed the PbI_2 phases passivation phenomenon of $CH_3NH_3PbI_3$ [54].

Another question is whether the two types of surface are stable under ambient conditions. Although the calculated surface energies suggest that the MAI-T surface is more stable than that of PBI_2-T surface, whether the surface MA^+ ions, which stays in the half-opened cages, can escape from the surface. Therefore, we took the five-layer models as examples and performed BOMD to simulate $CH_3NH_3PbI_3$ pervoskite surfaces at 300 K. The energy–time curves shown in Fig. 3 show that for the whole BOMD simulation of 15 ps, no energy jump occurs for either kind of surface. Thus, both MAI-T and PBI_2-T surface are thermodynamical stable at the room temperature.

3.3. The electronic properties

We investigated the electronic properties of two types of $CH_3NH_3PbI_3$ surfaces to provide further insight into their difference for photovoltaics. In order to know the effect of the thickness on the electronic properties, the band gaps for the

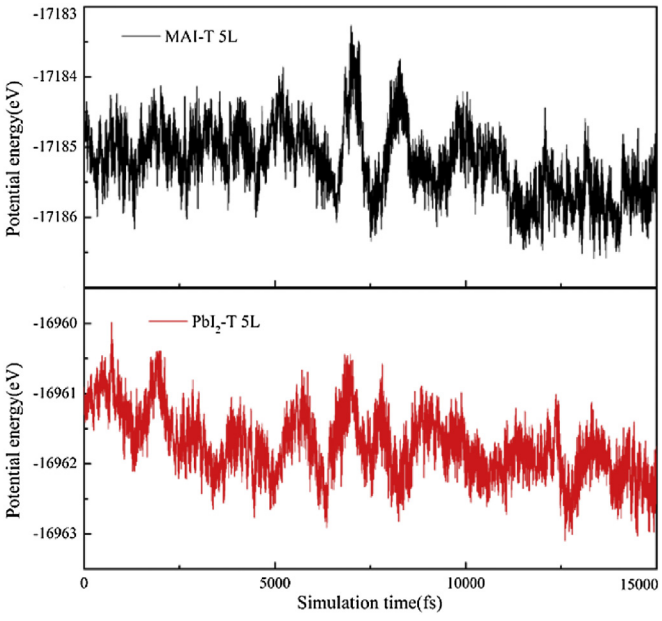

Fig. 3. The potential energy changes as a function of the simulation time during BOMD simulations for both terminations: (a) MAI, (b) PbI_2. The simulations were carried out with five-layer slabs for both terminations.

different numbers of layers are examined, as shown in Fig. 4. In our previous work, the band gap of bulk tetragonal phase $CH_3NH_3PbI_3$ was found to be about 1.6 eV (Fig. 4(b)) [53], which agrees with the experimental results. It is well-known that the spin–orbit coupling (SOC) effect has great effect on the calculated band gap, as shown in the previous work [29]. In order to check the effect of the SOC, we check the SOC effect on the band gap of bulk $CH_3NH_3PbI_3$. The calculated band gap is 0.60 eV, which is obviously smaller than the one with pure PBE. Interestingly, the band gaps of the different terminations exhibit the distinct feature. Firstly, the calculated band gaps of MAI-T slabs are sensitive to the thickness of the slab. With the increase of number of layers from single to five, the band gaps of MAI-T slabs gradually decrease from 2.46 eV to 1.69 eV, gradually approaching to that of the bulk material. It should be noted that the convergence of the band gap is very slow for the MAI-T type surface, and the band gap still does not fully converge for the 5-layer. While the further increase the number of layers should not affect the trend. On the other hand, the band gaps of PBI_2-T slabs are insensitive to number of layers with the values of about 1.4 eV, which are smaller than that of bulk material.

As shown in Fig. 4(c)–(f), the calculated band structures of both terminations suggest that the $CH_3NH_3PbI_3$ (001) is a direct band gap at the Γ point. However, the different terminations exhibit distinct band edge characteristics. As for bulk $CH_3NH_3PbI_3$ perovskites, the valence band maximum (VBM) is mainly contributed by *p* orbital of I atom and partly contributed by *s* orbital of Pb atom, while the conduction band minimum (CBM) is dominated by *p* orbitals of Pb atom. Although MAI-T slabs contains unsaturated surface I atoms, there is no obvious surface I states. As the number of layer increases, the position of CBM gradually shifts downward, resulting in the reduction of band gap. Different from the MAI-T, PBI_2-T slabs contain unsaturated Pb atoms on the surface. From the band structure of single-layer PBI_2-T slabs,

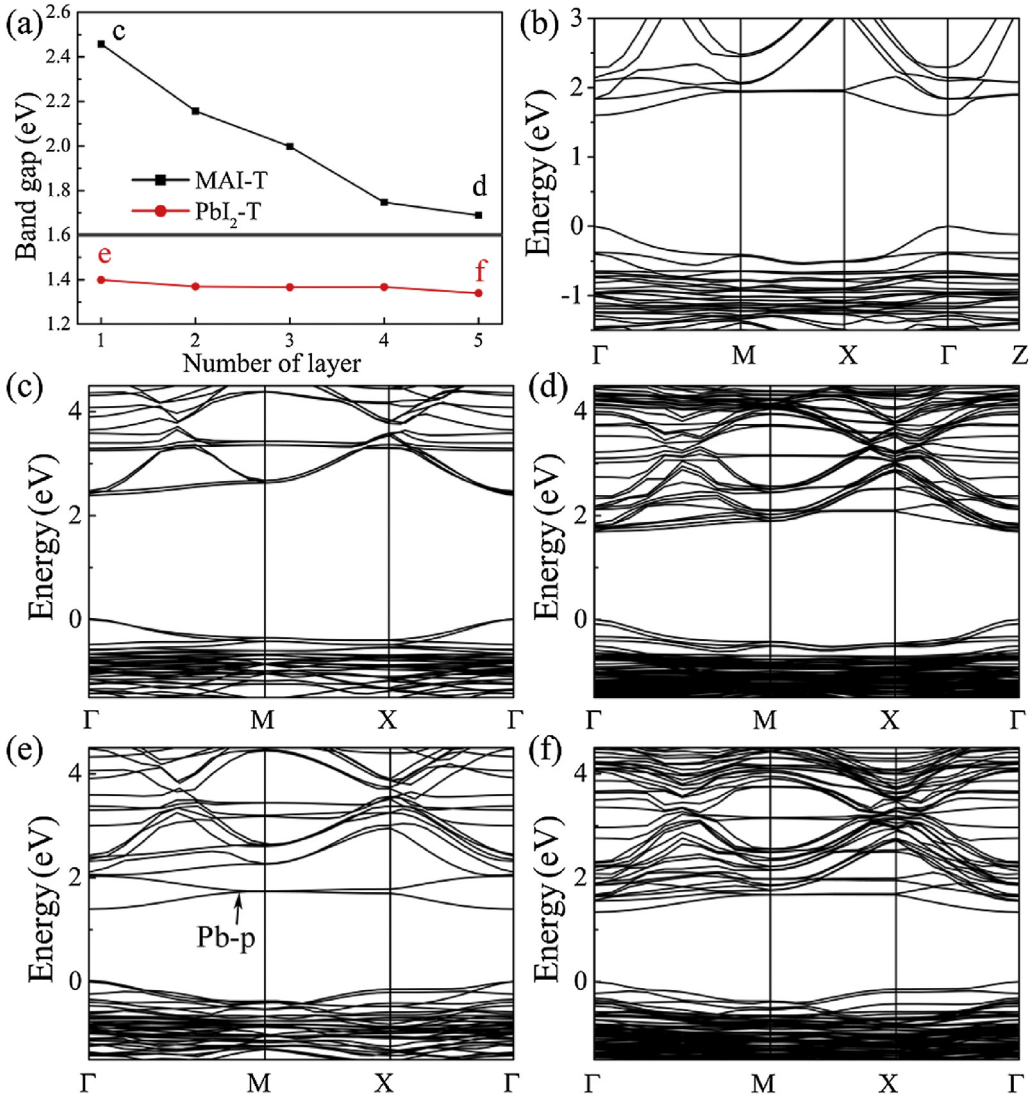

Fig. 4. (a) The calculated band gaps of the two different terminations (MAI-T and PBI_2-T) as a function of slab thickness. The calculated band structures of $CH_3NH_3PbI_3$ (b) bulk, (c) single layer MAI-T, (d) five layers MAI-T, (e) single layer PBI_2-T, (f) five layers PBI_2-T surfaces slabs, respectively.

the first and second CBM bands located at about 1.4 and 2.0 eV above the Fermi level at the Γ point are obviously different from that of MAI-T slabs. Between M and X point, the two CMB bands are almost flat and degenerate; and they split again along the path X−Γ. As the increase of the number of layers, the position of surface Pb bands is quite similar to that of single layer. Therefore, the band gap of PBI_2-T slabs hardly changes as the number of layers increases.

In order to understand the origin of the difference between the band structures of two surfaces, we analyzed the projected density of states (PDOS) of both types of one-layer slabs as shown in Fig. 5. There are two types of I atoms in the $CH_3NH_3PbI_3$ perovskites: axial I atoms with chemical bond along z direction and equatorial I atoms with chemical bond in xy plane. The VBM of MAI-T slab includes primary I-p_z, and partly I-p_x, I-p_y as well as Pb-s orbital, while that of PBI_2-T slab have no contribution from I-p_z, this is due to the surface of MAI-T slab have axial I atoms and surface of PBI_2-T slab have no axial I atoms. On the contrary, because the presence of dangling bonds of Pb-p_z orbital for PBI_2-T slab, the CBM of PBI_2-T slab are mainly Pb-p_z orbital, while CBM of MAI-T slab have hardly contribution from Pb-p_z orbital.

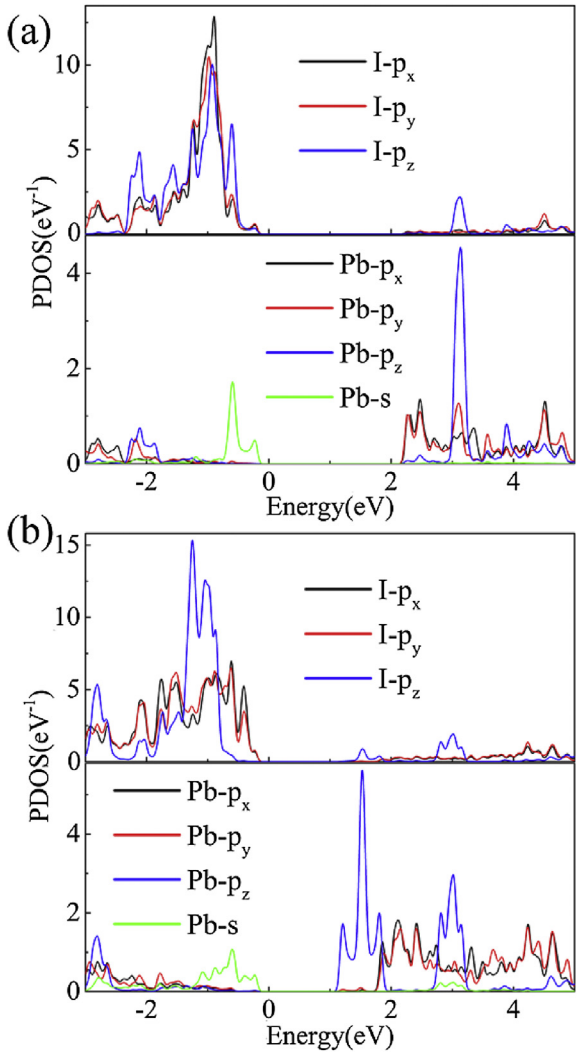

Fig. 5. The PDOS of the I and Pb atoms for one layer (a) MAI-T and (b) PBI_2-T slabs.

3.4. The optical properties

In order to know how the termination affects the optical properties, the detailed optical absorption coefficients of both types surface are calculated based on the Fermi golden rule (see Fig. 6). The complex dielectric function with the real and imaginary parts is used to describe the linear optical properties of the system. The imaginary part of the dielectric function represents direct inter-band transitions between occupied and unoccupied electronic states, and the real part can be obtained from with the Kramers−Kronig relations. The absorption coefficient can be obtained from real and imaginary parts of dielectric function. For MAI-T surface, two peaks are observed in the visible light region. The first peak redshifts from 2.5 eV for single layer to 2.2 eV for five layers, while the second peak located at about 2.7 eV remains unchanged as the number of layers increases. For PBI_2-T surface, the first peak slightly redshifts and the second peak are nearly at the same position. It should be noted that the calculated absorption coefficients for PBI_2-T slabs are higher than those of MAI-T slabs. As the number of layers increases, the difference gradually diminishes. The main reason is that the fundamental band gaps of the latter are larger than the former. As a result, the transition probability is reduced in the MAI-T surface according to the Fermi-Golden rule. These results indicate that $CH_3NH_3PbI_3$ pervoskites with PBI_2-T surfaces are more effective solar energy absorbers in the visible light spectrum.

4. Summary

In this work, two types of $CH_3NH_3PbI_3$ (001) surfaces are investigated by first-principles calculations. The results show that the MAI-terminated (MAI-T) and PbI_2-terminated (PbI_2-T) surfaces exhibit different stability and electronic properties. Although the two kinds of $CH_3NH_3PbI_3$ (001) are

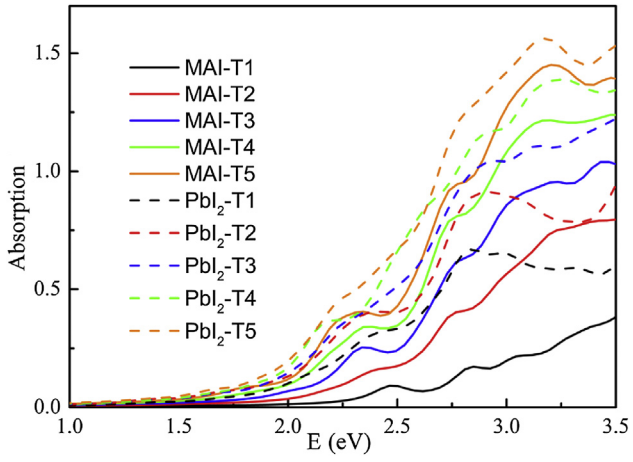

Fig. 6. Calculated absorption coefficients for the two terminations with the different slab thickness. Here, the solid lines represent MAI-T surfaces and dotted lines represent PBI_2-T surfaces.

both thermodynamical stable at room temperature, MAI-T is relatively more favorable than PBI_2-T in equilibrium growth conditions. The band gap of MAI-T reduces with the increase of slab thickness, but usually exhibits a relatively large value compared with the PbI_2-T. PbI_2-T show small band gaps than MAI-T due to the surface Pb state. The calculated optical absorption coefficients suggest that both terminations are effective solar energy absorbers in the visible light spectrum.

Acknowledgments

This work was supported by the National Natural Science Foundation of China (No. 51222212, No. 11447011), the MOST of China (973 Project, Grant No. 2011CB922200).

References

[1] Gao P, Gratzel M, Nazeeruddin MK. Organohalide lead perovskites for photovoltaic applications. Energy Environ Sci 2014;7:2448–63.
[2] Sum TC, Mathews N. Advancements in perovskite solar cells: photophysics behind the photovoltaics. Energy Environ Sci 2014;7:2518–34.
[3] Kojima A, Teshima K, Shirai Y, Miyasaka T. Organometal halide perovskites as visible-light sensitizers for photovoltaic cells. J Am Chem Soc 2009;131:6050–1.
[4] Im J-H, Lee C-R, Lee J-W, Park S-W, Park N-G. 6.5% efficient perovskite quantum-dot-sensitized solar cell. Nanoscale 2011;3:4088–93.
[5] Chung I, Lee B, He J, Chang RPH, Kanatzidis MG. All-solid-state dye-sensitized solar cells with high efficiency. Nature 2012;485:486–9.
[6] Kim H-S, Lee C-R, Im J-H, Lee K-B, Moehl T, Marchioro A, et al. Lead iodide perovskite sensitized all-solid-state submicron thin film mesoscopic solar cell with efficiency exceeding 9%. Sci Rep 2012;2:591.
[7] Burschka J, Pellet N, Moon S-J, Humphry-Baker R, Gao P, Nazeeruddin MK, et al. Sequential deposition as a route to high-performance perovskite-sensitized solar cells. Nature 2013;499:316–9.
[8] Liu M, Johnston MB, Snaith HJ. Efficient planar heterojunction perovskite solar cells by vapour deposition. Nature 2013;501:395–8.
[9] Zhou H, Chen Q, Li G, Luo S, Song T-b, Duan H-S, et al. Interface engineering of highly efficient perovskite solar cells. Science 2014;345:542–6.
[10] Malinkiewicz O, Yella A, Lee YH, Espallargas GM, Graetzel M, Nazeeruddin MK, et al. Perovskite solar cells employing organic charge-transport layers. Nat Photon 2014;8:128–32.
[11] Jeng J-Y, Chiang Y-F, Lee M-H, Peng S-R, Guo T-F, Chen P, et al. $CH_3NH_3PbI_3$ Perovskite/Fullerene planar-heterojunction hybrid solar cells. Adv Mater 2013;25:3727–32.
[12] Wang JT-W, Ball JM, Barea EM, Abate A, Alexander-Webber JA, Huang J, et al. Low-temperature processed electron collection layers of Graphene/TiO_2 nanocomposites in thin film perovskite solar cells. Nano Lett 2013;14:724–30.
[13] Lee MM, Teuscher J, Miyasaka T, Murakami TN, Snaith HJ. Efficient hybrid solar cells based on meso-superstructured organometal halide perovskites. Science 2012;338:643–7.
[14] Yella A, Heiniger L-P, Gao P, Nazeeruddin MK, Grätzel M. Nanocrystalline rutile electron extraction layer enables low-temperature solution processed perovskite photovoltaics with 13.7% efficiency. Nano Lett 2014;14:2591–6.
[15] Liu D, Kelly TL. Perovskite solar cells with a planar heterojunction structure prepared using room-temperature solution processing techniques. Nat Photon 2014;8:133–8.
[16] Wojciechowski K, Saliba M, Leijtens T, Abate A, Snaith HJ. Sub-150 [degree]C processed meso-superstructured perovskite solar cells with enhanced efficiency. Energy Environ Sci 2014;7:1142–7.
[17] Christians JA, Fung RCM, Kamat PV. An inorganic hole conductor for organo-lead halide perovskite solar cells. Improved hole conductivity with copper iodide. J Am Chem Soc 2013;136:758–64.
[18] Ito S, Tanaka S, Vahlman H, Nishino H, Manabe K, Lund P. Carbon-double-bond-Free printed solar cells from TiO_2/$CH_3NH_3PbI_3$/CuSCN/Au: structural control and photoaging effects. ChemPhysChem 2014;15:1194–200.
[19] Leijtens T, Stranks SD, Eperon GE, Lindblad R, Johansson EMJ, McPherson IJ, et al. Electronic properties of meso-superstructured and planar organometal halide perovskite films: charge trapping, photodoping, and carrier mobility. ACS Nano 2014;8:7147–55.
[20] Rong Y, Ku Z, Mei A, Liu T, Xu M, Ko S, et al. Hole-Conductor-Free mesoscopic TiO_2/$CH_3NH_3PbI_3$ heterojunction solar cells based on anatase nanosheets and carbon counter electrodes. J Phys Chem Lett 2014;5:2160–4.
[21] Leijtens T, Lauber B, Eperon GE, Stranks SD, Snaith HJ. The importance of perovskite pore filling in organometal mixed halide sensitized TiO_2-based solar cells. J Phys Chem Lett 2014;5:1096–102.
[22] Schulz P, Edri E, Kirmayer S, Hodes G, Cahen D, Kahn A. Interface energetics in organo-metal halide perovskite-based photovoltaic cells. Energy Environ Sci 2014;7:1377–81.
[23] Shi J, Dong J, Lv S, Xu Y, Zhu L, Xiao J, et al. Hole-conductor-free perovskite organic lead iodide heterojunction thin-film solar cells: high efficiency and junction property. Appl Phys Lett 2014;104:063901.
[24] Roldan-Carmona C, Malinkiewicz O, Soriano A, Minguez Espallargas G, Garcia A, Reinecke P, et al. Flexible high efficiency perovskite solar cells. Energy Environ Sci 2014;7:994–7.
[25] Chen Q, Zhou H, Hong Z, Luo S, Duan H-S, Wang H-H, et al. Planar heterojunction perovskite solar cells via vapor-assisted solution process. J Am Chem Soc 2013;136:622–5.
[26] Even J, Pedesseau L, Jancu J-M, Katan C. Importance of spin–orbit coupling in hybrid organic/inorganic perovskites for photovoltaic applications. J Phys Chem Lett 2013;4:2999–3005.
[27] Lang L, Yang J-H, Liu H-R, Xiang HJ, Gong XG. First-principles study on the electronic and optical properties of cubic ABX3 halide perovskites. Phys Lett A 2014;378:290–3.
[28] Filippetti A, Mattoni A. Hybrid perovskites for photovoltaics: insights from first principles. Phys Rev B 2014;89:125203.
[29] Umari P, Mosconi E, De Angelis F. Relativistic GW calculations on $CH_3NH_3PbI_3$ and $CH_3NH_3SnI_3$ perovskites for solar cell applications. Sci Rep 2014;4:4467.
[30] Amat A, Mosconi E, Ronca E, Quarti C, Umari P, Nazeeruddin MK, et al. Cation-induced band-gap tuning in organohalide perovskites: interplay of spin–orbit coupling and octahedra tilting. Nano Lett 2014;14:3608–16.
[31] Yin W-J, Shi T, Yan Y. Unique properties of halide perovskites as possible origins of the Superior solar cell performance. Adv Mater 2014;26:4653–8.
[32] Yin W-J, Shi T, Yan Y. Unusual defect physics in $CH_3NH_3PbI_3$ perovskite solar cell absorber. Appl Phys Lett 2014;104:063903.
[33] Mosconi E, Amat A, Nazeeruddin MK, Grätzel M, De Angelis F. First-principles modeling of mixed halide organometal perovskites for photovoltaic applications. J Phys Chem C 2013;117:13902–13.
[34] Agiorgousis ML, Sun Y-Y, Zeng H, Zhang S. Strong covalency-induced recombination centers in perovskite solar cell material $CH_3NH_3PbI_3$. J Am Chem Soc 2014;136:14570–5.
[35] Frost JM, Butler KT, Brivio F, Hendon CH, van Schilfgaarde M, Walsh A. Atomistic origins of high-performance in hybrid halide perovskite solar cells. Nano Lett 2014;14:2584–90.
[36] Ma J, Wang L-W. Nanoscale charge localization induced by random orientations of organic molecules in hybrid perovskite $CH_3NH_3PbI_3$. Nano Lett 2014;15:248–53.
[37] Quarti C, Mosconi E, De Angelis F. Interplay of orientational order and electronic structure in methylammonium lead iodide: implications for solar cell operation. Chem Mater 2014;26:6557–69.
[38] Haruyama J, Sodeyama K, Han L, Tateyama Y. Termination dependence of tetragonal $CH_3NH_3PbI_3$ surfaces for perovskite solar cells. J Phys Chem Lett 2014;5:2903–9.
[39] Kresse G, Hafner J. Ab initio molecular dynamics for liquid metals. Phys Rev B 1993;47:558–61.

[40] Kresse G, Furthmüller J. Efficient iterative schemes for ab initio total-energy calculations using a plane-wave basis set. Phys Rev B 1996;54:11169–86.
[41] Blöchl PE. Projector augmented-wave method. Phys Rev B 1994;50:17953–79.
[42] Kresse G, Joubert D. From ultrasoft pseudopotentials to the projector augmented-wave method. Phys Rev B 1999;59:1758–75.
[43] Blöchl P, Först C, Schimpl J. Projector augmented wave method:ab initio molecular dynamics with full wave functions. Bull Mater Sci 2003;26:33–41.
[44] Monkhorst HJ, Pack JD. Special points for brillouin-zone integrations. Phys Rev B 1976;13:5188–92.
[45] Dion M, Rydberg H, Schröder E, Langreth DC, Lundqvist BI. Van der Waals density functional for general geometries. Phys Rev Lett 2004;92:246401.
[46] Klimeš J, Bowler DR, Michaelides A. Chemical accuracy for the van der Waals density functional. J Phys Condens Matter 2010;22:022201.
[47] Klimeš J, Bowler DR, Michaelides A. Van der Waals density functionals applied to solids. Phys Rev B 2011;83:195131.
[48] Perdew JP, Burke K, Ernzerhof M. Generalized gradient approximation made simple. Phys Rev Lett 1996;77:3865–8.
[49] VandeVondele J, Krack M, Mohamed F, Parrinello M, Chassaing T, Hutter J. Quickstep: fast and accurate density functional calculations using a mixed Gaussian and plane waves approach. Comput Phys Commun 2005;167:103–28.
[50] VandeVondele J, Hutter J. Gaussian basis sets for accurate calculations on molecular systems in gas and condensed phases. J Chem Phys 2007;127:103–28.
[51] Goedecker S, Teter M, Hutter J. Separable dual-space Gaussian pseudopotentials. Phys Rev B 1996;54:1703–10.
[52] Kawamura Y, Mashiyama H, Hasebe K. Structural study on cubic–tetragonal transition of $CH_3NH_3PbI_3$. J Phys Soc Jpn 2002;71:1694–7.
[53] Geng W, Zhang L, Zhang Y-N, Lau W-M, Liu L-M. First-principles study of lead iodide perovskite tetragonal and orthorhombic phases for photovoltaics. J Phys Chem C 2014;118:19565–71.
[54] Chen Q, Zhou H, Song T-B, Luo S, Hong Z, Duan H-S, et al. Controllable self-induced passivation of hybrid Lead iodide perovskites toward high performance solar cells. Nano Lett 2014;14:4158–63.

Dr. Wei Geng, Beijing Computational Science Research Center Email: gengwei@csrc.ac.cn. Dr. Wei Geng received his B.S. in Chemistry (2006) and Ph.D. in Analytical Chemistry (2013) from Lanzhou University. He joined the Beijing Computational Science Research Center (CSRC) as a postdoctoral researcher in 2013. His recent research focuses on photovoltaic materials and nanocatalysts.

Dr. Li-Min Liu Beijing Computational Science Research Center Email: limin.liu@csrc.ac.cn. Dr. Li-Min Liu received his PhD degree in Materials Science from the Institute of Metal Research, Chinese Academy of Sciences, in 2006. During his PhD study, he visited Queen' University of Belfast, U.K., for a year. Then he worked in Fritz-Haber-Institut (Germany), University College London (U.K.), and Princeton University. Since 2012, he takes a tenure-track position in Beijing Computational Science Research Center. He has co-authored more than 80 journal papers. He was granted "1000-plan for the young talent" and "the National Science Fund for Excellent Young Scholars". His research interests focus on the nanocatalysts, TiO_2-based photocatalysis, and aqueous water solid interfaces for the electrocatalysis and fuel cell.